The Effects of Root Opening on Mechanical Properties, Deformation and Residual Stress of Weldments

Mechanical properties for multipass welds are investigated and weld deformation and residual stress are simulated using finite element analysis

BY G. B. JANG, H. K. KIM AND S. S. KANG

ABSTRACT. In steel bridge manufacturing, dimensional differences caused by weld deformation often occur because multipass welding is used to join thick plates. It frequently develops that root openings are out of tolerance at butt joints. For example, to be within tolerance, root openings must be controlled to below 6 mm for butt-joint welds in plates under 20 mm thick, but a root opening of 30 mm can develop in the field. In that case, a part 24 mm out of tolerance is generally built up. However, there has been no accumulated data and standards developed regarding these built-up welded parts. In the present case, a study was performed to accumulate data on the behavior of built-up parts and to verify the effects of root opening on the mechanical properties of the welded parts. For that purpose, tensile, bend, impact and hardness tests were carried out on weld specimens having 0-, 6- and 30-mm root openings. Additionally, the finite element common code (MARC) was used to study the effects of 0-, 6- and 30-mm root openings on residual stress and weld deformation in multipass welding. The results of the experiments and of the analysis were compared. In the analysis, a 100% ramp heat input model was used to avoid the numerical convergence problem caused by an instantaneous increase in temperature near the fusion zone. The effect of a moving arc in a two-dimensional plane was also included. Additionally, to ensure the accuracy of the analysis and to save time, small time increments were applied in a period with instantaneous temperature fluctuations, while large time increments were used in another period. The experimental and analytical results show good correlation. Weld-included residual stresses and deformation distribution of the specimen with the 30-mm root opening appeared to be asymmetric and the magnitude was larger than those of root opening specimens in tolerance.

G. B. JANG, H. K. KIM and S. S. KANG are with the Micro-Plasticity Laboratory in the Dept. of Mechanical Engineering, Pusan National University, Pusan, Korea.

Introduction

When steel structures are welded, a localized fusion zone is generated in the weld joint because of the high heat input from the arc, and then nonuniform temperature distribution through heat conduction is induced. Therefore, nonuniform heat deformation and thermal stress are included in the as-welded parts. As a result, plastic deformation is retained within the weldment and nonlinear plastic deformations and residual stresses exist after cooling of the welded joint (Refs. 1, 2). Many problems occur in the field because of dimensional differences that occur as a result of these weld deformations during manufacturing of large steel structures (Ref. 3). For thick-section welded steel bridges, many welders frequently neglect the occurrence of dimensional differences caused by the weld deformation that results from multipass welding. When an out-of-tolerance root opening arises from the dimensional difference through weld deformation, parts out of tolerance are built up in the field. While this phenomenon is common, building up the weld is usually performed without systematic inspection.

KEY WORDS

Multipass Welding
Root Opening
Residual Stress
Deformation
Sequential Thermal-Mechanical Analysis

Steel plate 15 mm thick is limited in practice to a root opening of less than 6 mm. However, dimensional differences caused by the weld deformation from heating and cooling of a localized fusion zone result in a root opening of greater than 6 mm to a maximum of 30 mm. In that case, after grinding, welding is performed to build up the weld by 24 mm in order to make a 6-mm root opening. There are difficulties, however, acquiring satisfactory data about problems that arise from this built-up weld and, furthermore, no standards exist regarding the built-up weld.

Although the built-up weld compensates for the dimensional difference in the root opening caused by weld deformation, it may impede work progress and create safety problems by lowering structural strength.

Many engineers have had difficulty in systematically quantifying weld residual stresses and deformations in large welded structures that use thick, welded steel plates (Ref. 4). Recently, finite element analysis has been used to quantify data about weld residual stresses and deformations (Refs. 5–7). However, it has emphasized single-pass welding rather than multipass welding. The effects of root opening size on weld residual stress and deformation have been analyzed using MARC, a software for finite element analysis (Ref. 8). The comparison between finite element analysis and experimental measurements through a systematic approach can be utilized as fundamental data for quantifying weld residual stresses and deformations for the design of welded steel structures (Refs. 9–12). In comparison with the existing heat-input model, this paper suggests a new model as an efficient analysis method for improving the accuracy of the solution and reducing analysis times.

Experimental Procedure and Welding Conditions

The steel, SWS 490A, used in this study is a hot-rolled steel utilized in the manufacture of bridges, vessels, automobiles, fuel storage tanks and other structures. It has excellent weldability. The chemical composition and mechanical properties of the base metal are shown in Tables 1 and 2. Welding was performed with the flux cored arc welding (FCAW) process. The welding wire used was SF-71. The shielding gas was an Ar-CO_2 mixture with a flow rate of 20–30 L/min. The test specimens had a 60-deg-angle V-groove. Their dimensions were 300 x 500 x 15 mm (2W x L x h). A cross section of the test specimen is shown in Fig. 1. The welding conditions for each specimen are shown in Tables 3–5. The surrounding atmospheric temperature was approximately 20°C, and postweld heat treatment was not applied.

In the experiments, butt-joint, multipass weldments with 0-, 6- and 30-mm root openings were manufactured with FCAW. Tensile, bend, impact and hardness tests were performed to evaluate mechanical performance. Moreover, microstructures were observed with an optical microscope. Charpy impact and Rockwell hardness tests were measured at distances 2.5, 7.5 and 12.5 mm from the upper surface of the specimens. To provide data for verification of the thermal analysis, thermocouples were placed on the specimens at node 84 (at a distance of 5 mm from the weld interface). After welding, a three-element, strain-gauge rosette was applied at a distance from the weld interface (Fig. 4), and the residual stresses were determined by using the hole-drilling method according to ASTM Standard E837. Lastly, weld deformation of the thickness direction was measured with a dial gauge. Dimension and shape of the experimental test specimen are shown in Fig. 2.

Finite Element Analysis

Finite Element Modeling and Mesh Generation

The coupling between the thermal and mechanical analyses takes place through

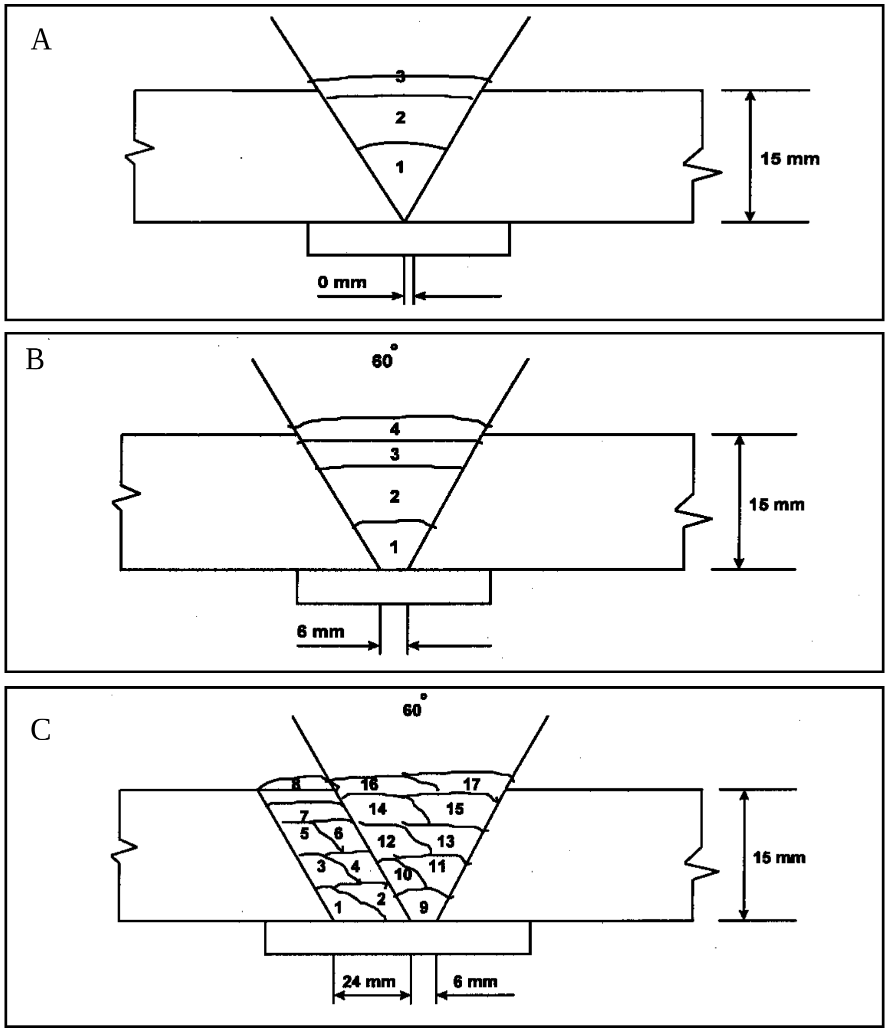

Fig. 1 — Schematic cross sections of the test specimens. A — 0-mm root opening; B — 6-mm root opening; C — 30-mm root opening built up with 24 mm of weld material to create a specimen with a 6-mm root opening (the numbers in each area of the weld zones represent the welding sequence of the multipass weld).

Table 1 — Chemical Composition of Base Metal

Material	Chemical Composition (wt-%)				
SWS	C	Si	Mn	P	S
490A	0.15	0.43	1.45	0.03	0.03

Table 2 — Mechanical Properties of Base Metal

Material	Mechanical Properties		
SWS	Yield Strength (N/mm^2)	Tensile Strength (N/mm^2)	Elongation (%)
490A	310	490 ~ 610	17

Table 3 — Welding Conditions for 0-mm Root Opening

Pass No.	Electrode Polarity	Diameter of Electrode	Ampere	Volt	Interpass Temperature	Weld Length (mm)	Time min	Time s	Speed (cm/min)	Heat Input (kJ/mm)
1	DCEP	1.4	220	26	Ambient	580	4	7	14.1	2.4
2	DCEP	1.4	230	27	94	610	3	30	17.4	2.1
3	DCEP	1.4	210	27	66	610	4	6	14.9	2.3
		Backgouging								
4	DCEP	1.4	190	26	45	560	3	15	17.2	1.7

RESEARCH/DEVELOPMENT/RESEARCH/DEVELOPMENT/RESEARCH/DEVELOPMENT

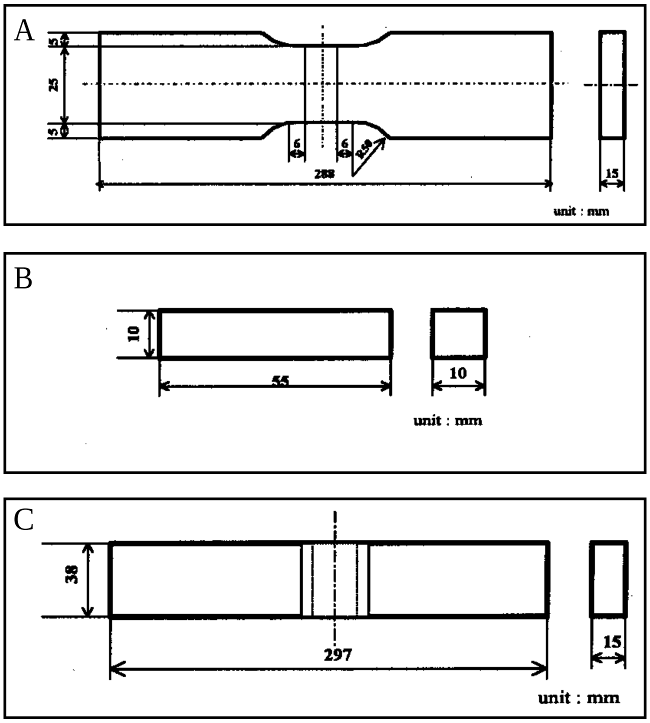

Fig. 2 — Dimensions and shape of the test specimens. A — Tensile specimen; B — impact specimen; C — bend specimen. (Test specimens were acquired in a perpendicular direction to the weld interface.)

the temperature-dependent material properties in the mechanical stress problem, which serves as input for heat transfer analysis. Additionally, a change in the temperature distribution contributes to deformation of the body through thermal strains and influences the material properties. Through this process, sequential thermal-mechanical analysis, from which the temperature distribution, stress and displacements induced by the thermal strain were obtained, was performed (Refs. 13, 14). Of course, all mechanical and thermal material properties may be temperature dependent and the governing matrix equations may be expressed as the following (Ref. 8):

$$M + D(T) + K(T)u = f \quad (1)$$

$$C(T) + K(T)T = Q + Q1 \quad (2)$$

where M is the mass matrix, C(T) is the specific heat matrices, K(T) is the thermal conductivity matrices, D(T) is the temperature-dependant displacement matrices, T is the nodal temperature vector, u is the displacement vector, f is the plastic work and Q1 is the amount of heat generated because of the plastic work.

The characteristics of the weld analysis require a large amount of time and storage memory to model the weld fusion and heat-affected zones. In the case of a single-pass weld, 3-D analysis that considers moving heat sources can be used, while for a multipass weld it is important to know many engineers tried to simplify the problem because of the difficulty of 3-D analysis. In this study, the assumption the cross section of each specimen has the same temperature distribution was used to predict the weld residual stresses and deformations during multipass welding of thick plates. A vertical cross section of the weld interface was used for 2-D analysis. In other words, the assumption of plain strain is utilized to consider the stress of the thickness direction to avoid

Table 4 — Welding Conditions for 6-mm Root Opening

Pass No.	Electrode Polarity	Diameter of Electrode	Ampere	Volt	Interpass Temperature	Weld Length (mm)	Time		Speed (cm/min)	Heat Input (kJ/mm)
							min	s		
1	DCEP	1.4	210	26	Ambient	620	5	51	10.6	3.1
2	DCEP	1.4	230	27	114	640	3	35	17.9	2.1
3	DCEP	1.4	230	29	111	660	4	41	14.1	2.8
4	DCEP	1.4	210	30	42	570	5	43	10.0	3.8

Table 5 — Welding Conditions for 30-mm Root Opening

Pass No.	Electrode Polarity	Diameter of Electrode	Ampere	Volt	Interpass Temperature	Weld Length (mm)	Time		Speed (cm/min)	Heat Input (kJ/mm)
							min	s		
1	DCEP	1.4	180	26	Ambient	620	4	6	15.1	1.9
2	DCEP	1.4	180	27	123	620	3	54	15.9	1.8
3	DCEP	1.4	200	27	72	620	3	7	19.9	1.6
4	DCEP	1.4	200	27	89	620	3	48	16.3	2.0
5	DCEP	1.4	200	27	120	620	3	6	20.0	1.6
6	DCEP	1.4	200	27	128	620	3	54	15.9	2.0
7	DCEP	1.4	200	26	133	620	2	50	21.9	1.4
8	DCEP	1.4	200	26	87	620	3	17	18.9	1.7
	Welding after grinding									
9	DCEP	1.4	180	26	62	620	7	12	8.6	3.3
10	DCEP	1.4	210	28	162	620	1	45	35.4	1.0
11	DCEP	1.4	220	28	135	620	2	0	31.0	1.2
12	DCEP	1.4	220	28	75	620	3	29	17.8	2.1
13	DCEP	1.4	210	28	63	620	4	30	13.8	2.6
14	DCEP	1.4	210	28	110	620	3	20	19/8.6	1.9
15	DCEP	1.4	210	28	120	620	3	38	17.1	2.1
16	DCEP	1.4	210	28	60	620	3	59	15.6	2.3
17	DCEP	1.4	210	28	103	620	4	9	14.9	2.4

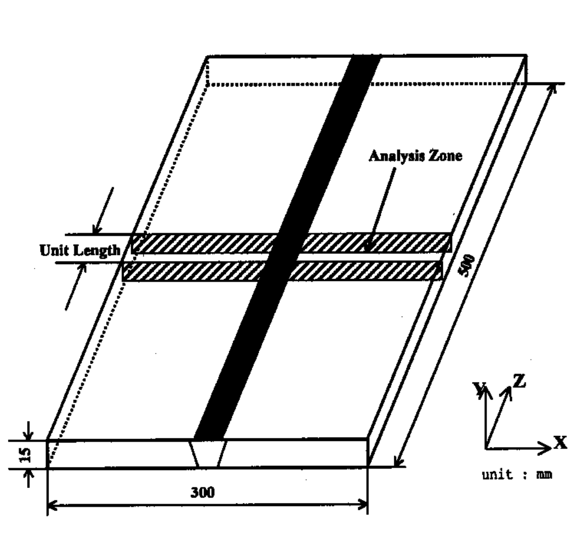

Fig. 3 — Schematic of the weld specimen and analysis zone showing the dimensions.

errors by generating excessive stress in the thickness direction if the multipass weld is analyzed as plain stress to predict residual stresses. The analysis model of the size of the weld specimen and vertical cross section passing unit length of the weld interface is presented in Fig. 3.

Localized heat input creates a fine mesh around the weld zone, which has an abrupt temperature gradient, and the size of the elements at a distance far from the weld fusion and heat-affected zones is increased to reduce analysis time. The node numbers for the analysis results and finite element model are presented in Fig. 4. The mesh for analysis is comprised of a four-node quadrilateral element and deactivated element in the weld joint.

Deactivate options deactivate elements except for the first of the multiple layers. When an element of the weld zone is deactivated, it does not contribute to stiffness and internal force. When an element is reactivated after welding of the first layer, it will have the stress level from when it was deactivated. The iterated process is performed continually until formation of the weld bead is complete. When the 24-mm built-up area is welded, a connected region as a nonbuilt-up mesh is deactivated to increase the accuracy of the deformation analysis. For this study, after the 24-mm buildup was finished, analysis methods were used that reactivated a connected nonbuilt-up mesh of 6 mm.

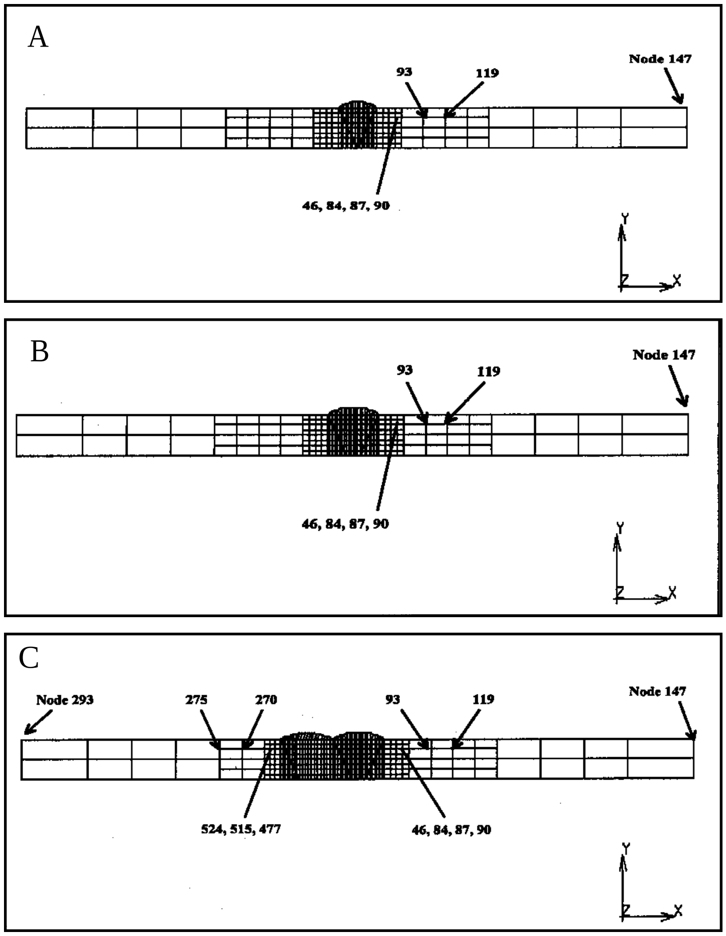

Fig. 4 — Mesh generation and node numbers. A — Model of a 0-mm root opening specimen that uses 272 elements and 304 nodes; B — model of a 6-mm root opening specimen that uses 326 elements and 364 nodes; C — model showing a 24-mm buildup and 6-mm root opening. It uses 489 elements and 534 nodes. The node index made at the beginning of a model is a measurement position for thermal cycle, residual stress and displacement. (Distance from weld interface of nodes 46, 84, 87, 119 and 147 is 2, 5, 8, 24 and 140 mm, respectively. Distance from the weld interface of nodes 477, 524, 275 and 293 is 2, 8, 20 and 118 mm, respectively. The distance from the surface is 4 mm.)

Boundary Conditions

The initial temperature of all nodes was 20°C, which was equivalent to atmospheric temperature. The nonlinearity in the analysis includes temperature-dependent properties, latent heat (phase change) effects, heat convection in the flow direction and nonlinear boundary conditions. In turn, temperature distributions can be used to generate thermal loads in a stress analysis. The thermal expansion coefficient, elastic modulus and yield strength as mechanical properties of material and heat convection coefficient, heat conduction coefficient and specific heat were input as a function of temperature in order to consider variations in material properties. Weld heat is lost to the surrounding atmosphere through convection and radiation, and radiation losses are greatest close to the weld pool. At some distance from the weld pool, convection is the primary mechanism for heat loss to the atmosphere. The effects on latent heat through phase change from solid to solid and solid to liquid were considered during welding. The material is isotropic and its yield behavior is applied by Von Mises' yield criteria.

The nodes in the center of the bottom surface were perfect as the boundary conditions required for mechanical analysis of the 0- and 6-mm root opening weldments. Since the specimen was welded under a condition where it lifted up at the steel or ceramic plates, the nodes of the region contacted at the plates were limited to the thickness direction (+y-direction). The center nodes of the upper surface were constrained because the 0-mm root opening sample was finished after the third pass and then backgouged. Finally, the 24-mm specimen was restricted at the center region of the built-up and 6-mm weld area. The weld zone lifted up at the steel or ceramic plates was restricted in a similar way.

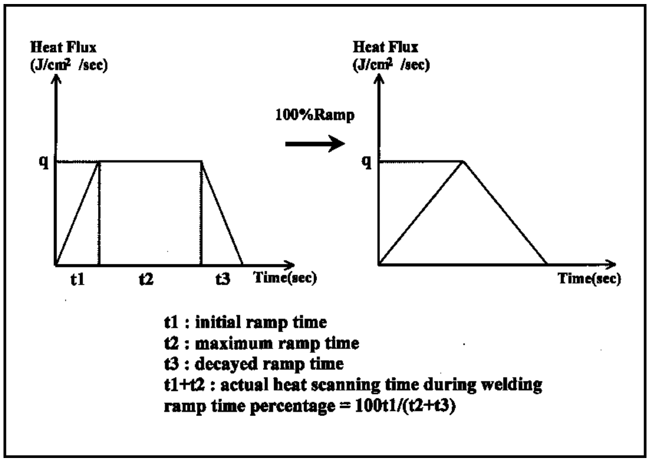

Fig. 5 — Shape of ramp heat input function. The area under the ramp function curve was kept constant to maintain the same net heat input energy and to study the effect on thermal and stress responses.

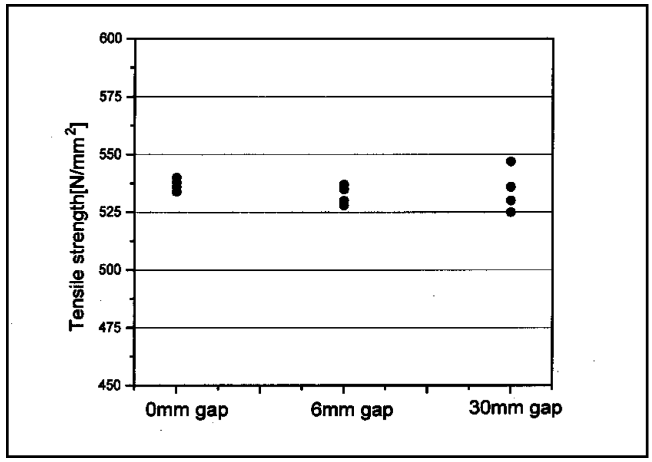

Fig. 6 — Plot of the tensile strength of each weld specimen.

Heat Input Model

It is important that heat input from the arc is exactly duplicated in modeling because the heat input model has an important effect on the accuracy of analysis from the temperature distribution, cooling rate, size of fusion zone and heat-affected zone to the strength of the weldment. The heat input model for analysis of weld residual stresses and deformations was distinguished as a ramp heat input model and a lumped pass model. A ramp heat input model was developed to avoid numerical convergence problems because of an instantaneous increase in temperature near the fusion zone, and enabled the model to include the effect of a moving arc in a 2-D plane. It takes into account the variation of plane energy flow in a 2-D model as the arc approaches, travels across and departs from each plane under investigation.

The lumped pass model for thick multipass welds developed to reduce analysis times and costs is useful in predicting residual stress, but it is troublesome in predicting weld deformation. In a single-V groove, the center of the total shrinkage force does not coincide with the neutral axis because the bead deposits are not symmetric about the neutral axis. This results in larger bend stress and produces different final stress or strain rates. The lumped pass amplifies these effects, so the ramp heat input model is recommended for welds that have unsymmetrical bead depositions such as a single-V-groove weld. The level is particularly severe in cases that have many weld passes such as the 30-mm root opening weld in this study.

As previously described, the following heat input model is used to reduce calculation costs and times through the ramp heat input model in this study. Small time increments are applied to a period of instantaneous temperature fluctuation that generates stiff temperature gradients due to the localized high heat input and rapid cooling near the fusion zone; large time increments are applied for other periods. Next, 100% ramp ratio is provided to improve the convergence of the analyses. These methods make a difference between the total time of actual welding and the analytical one, including cooling time. Figure 5 shows the heat input model of the 100% ramp ratio.

In other words, the interpass temperature (the temperature to which the weld region cools between passes) exists in the actual weld. The total weld time is the sum of the welding time of each layer and the cooling time required for each interpass temperature. However, if ramp ratio is increased to improve analyses, the total time of analysis is greater than the actual welding time. Therefore, this time difference must be considered in the analysis. The heat input rates of the 2-D analysis are given by the surface flux and expressed as the following:

$$Q = \eta EI/bL \qquad (3)$$

where η represents 0.8 as the arc efficiency, E and I are arc volts and amperes, and b and L represent the width of the weld bead and the length of the weld direction of the heat input region, that is, unit length at the 2-D analysis, respectively.

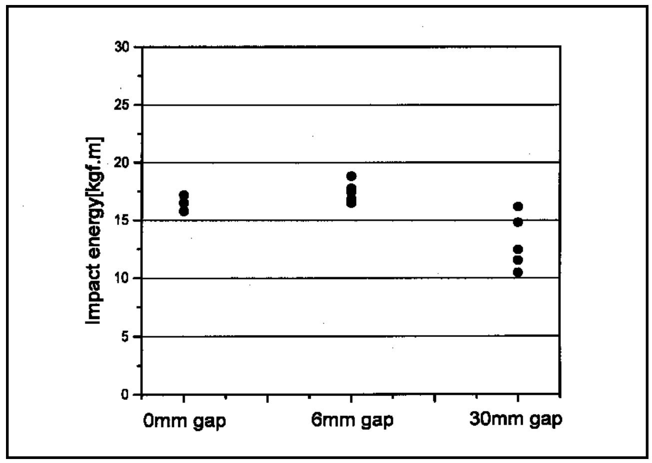

Fig. 7 — Plot of the impact energy of each weld specimen.

Results and Discussion

Experimental Results and Considerations

Tensile test results for each specimen are presented in Fig. 6. The figure shows approximately 534–540 MPa for the 0-mm root opening, 528–537 MPa for the 6-mm root opening and 536–547 MPa for the weld with the 24-mm buildup and 6-mm root opening. In total, the differences are not large. The tensile strengths for each specimen were shown to be satisfied because fractures were generated in the base metal, not the weld metal. The 30-mm root opening weldment had sufficient static strength, but dynamic strength such as impact and fatigue strength may be insufficient. For that reason, large scattered tensile tests were suggested because of the size of the weld pool and fusion zone. The bend test for each specimen was performed four times, and the criteria of no cracks was satisfied for each specimen. Bend test results are presented in Table 6.

Figure 7 shows the impact energy of each weld specimen. There is no difference between the impact energy of the welds with 0- and 6-mm root openings. In the case of the 30-mm root opening, it is assumed the large scatter between the measured data is because of the effects of an enlarged heat-affected zone caused by high heat input. Consequently, it is expected the 30-mm root opening weldment will have a problem with dynamic strength such as fatigue strength because of the nonuniformity of its tensile strength and impact values.

The results of the hardness measurement are presented in Fig. 8A–C. Hardness was measured at 2.5, 7.5 and 12.5 mm from the upper surface of the specimens. The hardness of the 0- and 6-mm root opening weldments showed little difference. In the case of the weldment with a 30-mm root opening, which was out of tolerance, the total hardness is slightly lower than that of the other welds.

Microstructures were acquired for each weld specimen. For the 0-mm root opening weld, the microstructure of the weld zone is nonuniform because of the effects of the multiple passes. An inherent segregation structure of the weld and a finely diffused region caused by multipass welding were observed. The microstructure of the heat-affected zone showed high heat input and the elimination of the initial hot-rolled structure. The lower and upper portions of the weld zone showed severe coarseness and segregation of the microstructure. Because the heat of welding in the lower portion of the weld zone transferred to the supporting plate with ease, weld heat caused only a small effect. The solidification structure is also retained because of the small effect of weld heat in the upper weld zone, which is filled with filler metal.

The microstructure of the weld with the 6-mm root opening was slightly different from that with the 0-mm root opening. Since the width of the weld cross-section, which was filled with all-weld metal in the upper portion, was increased by 21 mm, the solidification structure of the welded layer disappeared because of the relatively greater heat input. However, that of the welded upper layer was widely distributed. This result is equivalent to the fact that the hardness of the upper solidified structure appears high, that is, despite the coarseness of the structure, the hardness is relatively widely distributed because of the existence of a martensitic structure due to rapid cooling.

Table 6 — Result of Bend Test

Welding specimen	Test times	Crack occurrence	Criterion
0-mm root opening	3	No	satisfaction
6-mm root opening	3	No	satisfaction
30-mm root opening	3	No	satisfaction

For the 30-mm root opening specimen, solidified structures and refined regions by heat appear as a nonuniform structure. Since the solidified structures are not dissolved by the weld heat, but are instead retained, they may have a problem if used in steel fabrications. This phenomenon may lead to the 30-mm root opening specimen being less reliable because of deterioration of the weld-included parts.

Analysis Results

Analysis of Thermal Cycle

The results of the analysis of the temperature cycle for different positions (note the node index in Fig. 3) of the width direction (x-direction) from the weld interface and a 4-mm distance from the surface is represented in Fig. 9. The 0- and 6-mm root opening welds are presented in Fig. 9A, B. The thermal cycle of the buildup area and the actual weld in the 30-mm root opening specimen are presented in Fig.

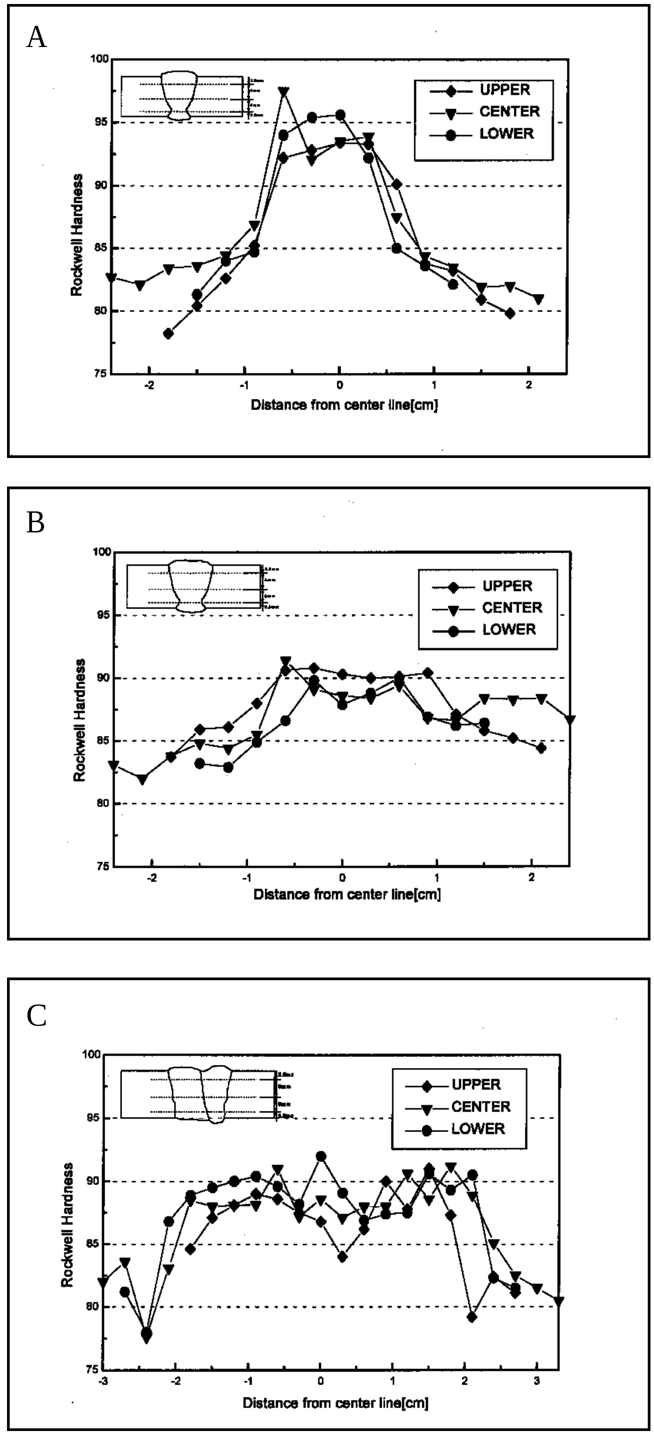

Fig. 8 — Comparison of the results and measured position of the hardness tests. A — 0-mm root opening weld specimen; B — 6-mm root opening specimen; C — weld specimen with a 24-mm buildup and 6-mm root opening.

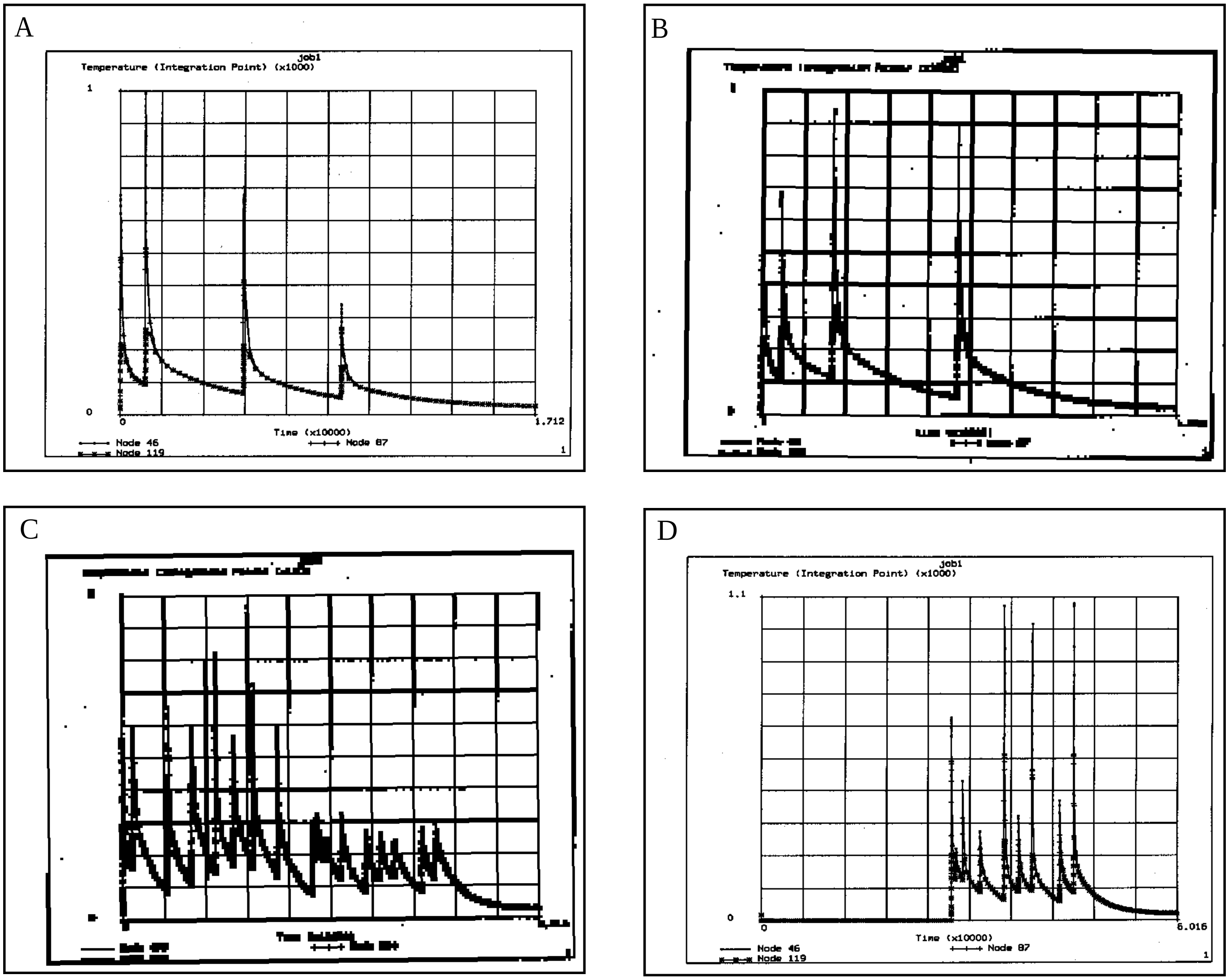

Fig. 9 — Comparison of the thermal cycles at various locations of each weld specimen. A — 0-mm root opening; B — 6-mm root opening; C — left side after 24-mm buildup and 6-mm root opening weld; D — right side after 24-mm buildup and 6-mm root opening weld. (Horizontal axis: time [s x 10000], vertical axis: temperature [°C x 1000].)

9C, D. The higher the peak temperature of the thermal cycle, the more it measures the position approach in the weld interface. Figure 10 shows a comparison between measured and analyzed results of the thermal cycle of the initial pass at the position (node number 84 of each test specimen) at which thermocouple was installed for the 0- and 6-mm welds and the 6-mm root opening weld after 24-mm of buildup. The analyzed data shows the measured temperature cycle is biased to the right side, and the peak temperature of the built-up weld is higher because of a more elongated weld time through the 100% ramp, as shown in Fig. 5. However, it shows some of the thermal cycles are very similar to others.

The equilibrium temperature (without differences in temperature in the various positions during the cooling process) is about 47°C for the 0-mm root opening and 48°C for the 6-mm root opening. For these two cases, the equilibrium temperature differed little because the number of passes and total heat input was nearly equal.

The equilibrium temperature after the 24-mm buildup was approximately 62°C — Fig. 9C, D. In this case, there were situations in which heat was not transferred to the right plates. The equilibrium temperature reached approximately 40°C after the 24-mm buildup and 6-mm root opening weld. The heat was transferred only to the left plate, but not the right one, when the buildup weld was performed. It shows equilibrium temperature is lower for the within-tolerance specimen because of the asymmetric heat transfer to the right plate when the 6-mm root opening weld is performed. The lower equilibrium temperature means cooling velocity is rapid. Consequently, the maximum value of retained stress is high when cooling velocity is slow. This can be verified by evaluation of residual stresses.

Residual Stress Evaluation

A weldment is locally heated, therefore, temperature distribution is not uniform, and structural and metallurgical changes take place in the joint during multipass welding. The weld metal and heat-affected zone immediately adjacent to the weld are at temperatures substantially above that of the unaffected base metal. As the weld zone solidifies and shrinks, it begins to exert stress on the surrounding weld metal and heat-affected zone. Because of that process, the retained Von Mises' equivalent stress after cooling of the three types of welds is retained in the weld metal and listed in

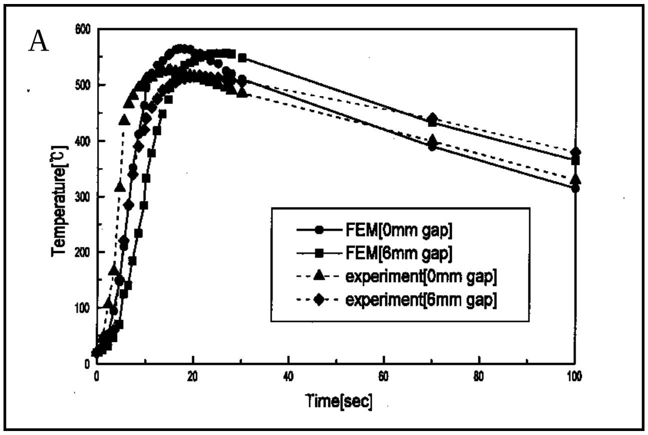

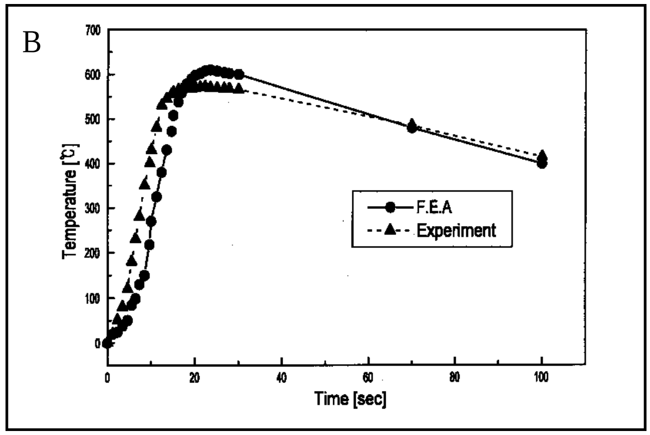

Fig. 10 — Comparison between measured and analyzed results of the thermal cycle. A — 0- and 6-mm root opening weld specimen; B — 30-mm root opening weld specimen.

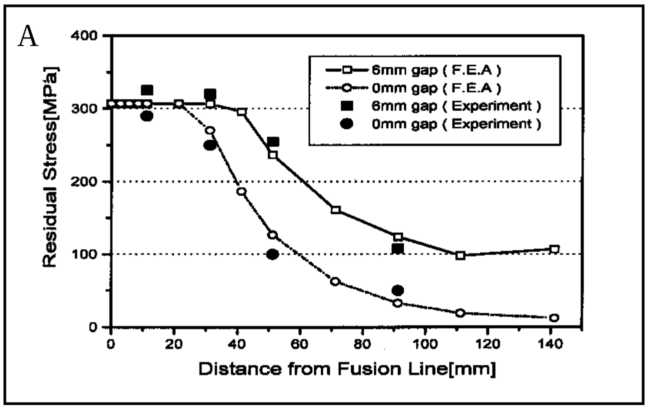

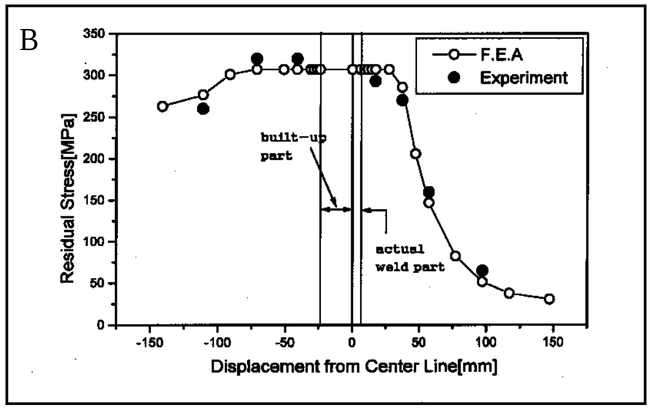

Fig. 11 — Comparison of the residual stress distribution by analysis and experiment. A — 0- and 6-mm root opening weld specimen; B — 30-mm root opening weld specimen.

Fig. 11. This shows the measured values of the experiment and analysis coincide well. The maximum Von Mises' equivalent stress for the 0- and 6-mm root opening welds is approximately 307 MPa, and it is concentrated symmetrically at the weld metal and heat-affected zone of the workpieces. The initial weld passes preheat the base metal of multipass welds. The effects are greatest on the second pass. As the preheating conditions after the second pass are stabilized, the resultant change in thermal cycle and cooling rate is less significant. However, final welding of the bottom surface after backgouging followed by the third pass leads to considerable reduction of the residual stress and deformation contrary to the others as shown in Fig. 11A. As a result, when plates with a long, thick butt joint are welded, welding of the bottom surface after backgouging can be used to reduce the residual stresses and deformation of the welded plate.

For the 6-mm root opening weld without backgouging, the maximum residual stress is distributed in a wide range because of the large weld pool. In the 24-mm buildup with a 6-mm root opening weld, the residual stress after cooling is retained as an asymmetric type and biased to the buildup weld as shown in Fig. 11B), because heat is not uniformly transferred to the plates. Since the final equilibrium temperature is lower than in the specimens within tolerance, the maximum Von Mises' equivalent stress is higher than that of the 0- and 6-mm root opening welds.

Weld Deformation Evaluation

The deformation of thickness direction (y-direction) after cooling followed by the final pass is shown in Fig. 12. These results show the measured values in the experiments and analysis coincide well. For the 0-mm root opening specimen, a small drop in angular deformation was generated when the final pass was performed on the bottom surface after backgouging, but this value was infinitesimal. For the 6-mm root opening specimen, general types of angular deformation typical in a butt weld showed displacement was limited to weld deformations of less than 1 mm by keeping the interpass temperature under 200°C. Weld deformation for the 24-mm buildup, 6-mm root opening specimen was opposite to the others. The buildup weld generated a positive angular deformation, and the 6-mm weld after buildup generated a negative angular deformation, that is, a drop due to sudden expansion because of high heat input.

To verify a history of weld deformation, the displacement of thickness (y-direction) and width (x-direction) at the edge of the upper surface (node number 147) is shown in Fig. 13. The horizontal axis is time (s) and the vertical axis is displacement of the thickness direction (cm). Displacement in the thickness direction after the final pass subsequent to backgouging approached zero in the case of the 0-mm root opening because of iteration of expansion and contraction — Fig. 13A. The instantaneous lifting that occurred with the heat input of the final pass followed by backgouging was at the bot-

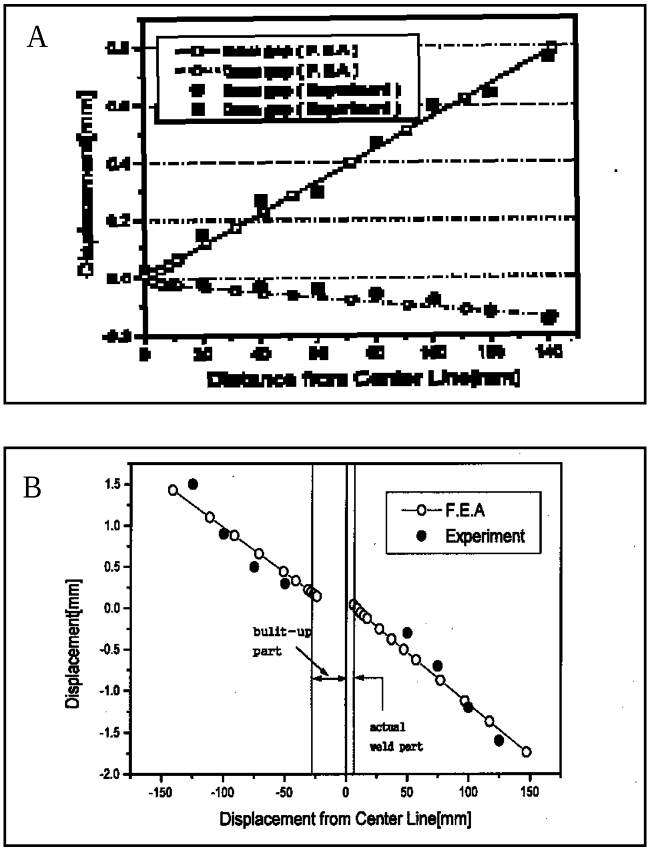

Fig. 12 — Comparison of the displacement of the thickness direction (y-direction) by analysis and experiment. A — 0- and 6-mm root opening weld specimen; B — 30-mm root opening weld specimen.

tom surface, and then there was a drop because cooling occurred. As a result, angular deformation approaches zero.

For the 6-mm root opening (Fig. 13B), there was a large displacement in the thickness direction after the final pass as a result of the high heat input from the final pass. Asymmetric deformation behavior (node number 293 and 147) is shown in Fig. 13C. Displacement of the thickness direction at node 239, which was generated by the buildup weld, was maintained without change until the final situation. Weld deformation, which had stayed at zero at node 239 during buildup welding, occurred suddenly after the 6-mm weld. In particular, considerable deformation was observed in the initial pass of the 6-mm weld. Finally, angular deformation dropped because of asymmetric heat transfer.

Conclusions

The following results were obtained through comparison of the finite element analysis and experimental data.

According to the tensile tests, tensile strength is approximately 534–540 MPa for the 0-mm root opening, 528–537 MPa for the 6-mm root opening and 536–547 MPa for the 30-mm root opening. There is little difference in the results, but in the case of the 30-mm root opening weld, the scatter in the tensile strength data is higher than for the other welds because of the extensive weld fusion zone and weld pool. Since no crack propagation was observed for each specimen, the results of the bend tests were satisfactory. According to the impact tests, there was little difference in the 0- and 6-mm root opening welds, but the scatter of impact values for the 30-mm root opening weld was higher and nonuniform. In terms of microstructure, refined regions resulting from weld heat and solidification that were not dissolved by the heat but were retained, appeared as a nonuniform structure. With regard to mechanical properties, it appears there are problems in attaining toughness. The static strength such as tensile and bend strength in the 24-mm buildup weld should have no problems in manufacturing structures, such as the steel bridges. However, there may be problems in reliability of the weldment as a result of reductions in toughness because of nonuniformity in the deteriorated regions of the weldment.

The residual stress is distributed symmetrically, and maximum value is the

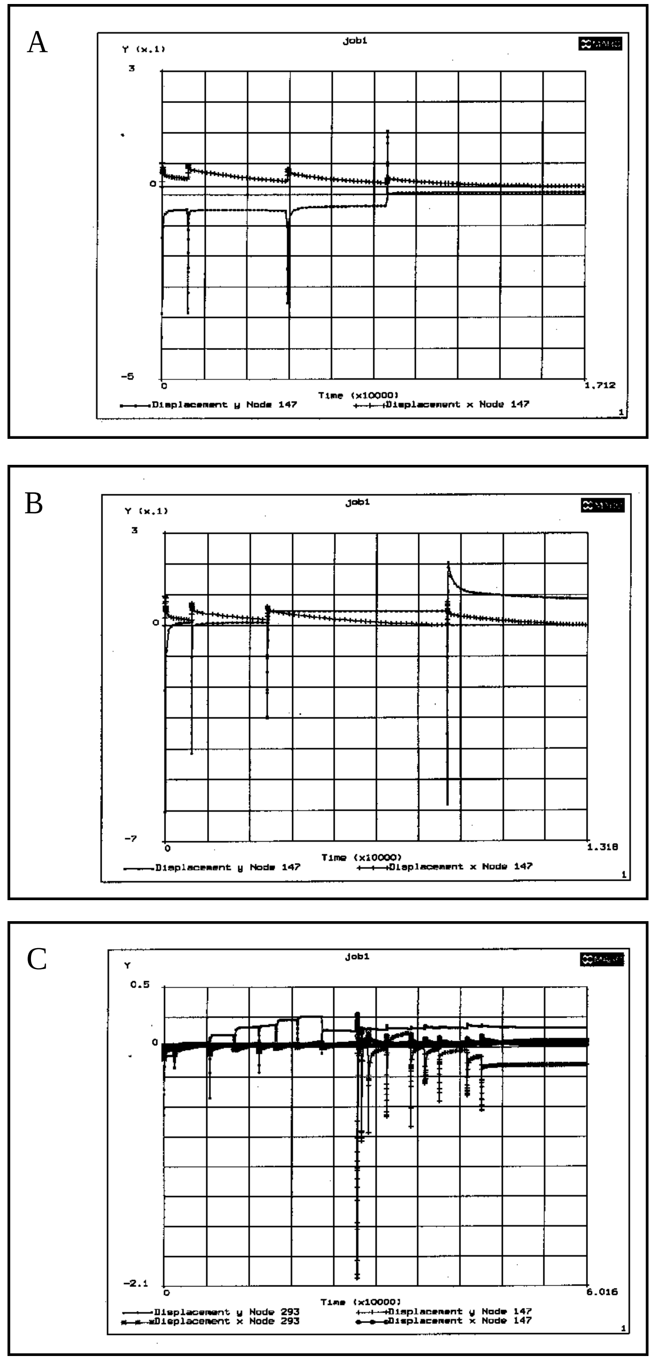

Fig. 13 — Comparison of the relation between displacement and time for each weld specimen. A — 0-mm root opening weld specimen; B — 6-mm root opening weld specimen; C — 24-mm buildup and 6-mm root opening weld specimen. (Horizontal axis: time [s x 10000]; vertical axis: displacement [cm].)

same for the 0- and 6-mm root opening welds. In the case of the 30-mm root opening weld, the equilibrium temperature is lower than the within-tolerance specimens and the distribution of the residual stress extends over a wide range asymmetrically because of the buildup weld. It might have a problem in dynamic strength because most of the residual stress is biased toward the built-up weld part.

Displacement in the thickness direction after the final pass followed by backgouging has little effect in the case of the 0-mm root opening. In the case of the 6-mm root opening weld without backgouging, a little angular distortion occurs, but the level of deformation is small. Therefore, there is no problem for the specimens within tolerance. However, in the case of the 30-mm root opening weld, the angular deformation in the asymmetric region where the side of the built-up weld is lifted up and the other side is dropped is greater than the other specimens.

In this study, the predicted weld residual stress and deformation as calculated from finite element analysis are found to be in close agreement with the experimental data.

References

1. Masubuchi, K. 1980. *Analysis of Welded Structure*. Pergamon Press.
2. Masubuchi, K. 1991. Recent research activities at MIT on residual stresses and distortion in welded structures. *Welding Journal* 70(12): 41–47.
3. Shibata, N. 1991. Prevention and estimation of welding deformation —thick plates steel structure (steel bridge). *JWS* 60(6): 20–25.
4. Natume, M. 1983. Weld distortion control on steel bridges and steel structures. *JWS* 52(8): 30–40.
5. Mahin, K. W., Winter, W., and Hoden, T. M. 1991. Prediction and measurement of residual elastic strain distribution in gas tungsten arc welds. *Welding Journal* 70(9): 245-s to 260-s.
6. Shim, Y., Feng, Z., Lee, S., Kim, D., Jaeger, J., Papritan, J. C., and Tsai, C. L. 1992. Determination of residual stresses in thick-section weldments. *Welding Journal* 71(9): 305–312.
7. Free, J. A., and Poter Goff, R. F. D. 1989. Predicting residual stress in multi-pass weldments with the finite element method. *Computer and Structures* 32(2): 365–372.
8. MARC User's Manual. 1996. Analysis Research Corp.
9. Shim, Y., Feng, Z., Lee, S., Kim, D., Jaeger, J., and Tsai, C. L. 1991. Modeling of welding residual stresses. *Proceedings of the Winter Annual Meeting of the ASME*, pp. 29–41.
10. Leung, C. K., and Pick, R. J. 1990. Finite element analysis of multipass welds. *WRC Bulletin 356*, pp. 11–33.
11. Ueda, Y., Takahashi, E., Fukuda, K., and Nakacho, K. 1974. Transient and residual stresses in multi-pass welds. *Transactions of JWRI* 3(1): 59–67.
12. The Ohio State University. 1992. Experimental verification of finite element modeling procedures for thick plates. Technical report submitted to U.S. Army Corps of Engineers Department of Welding Engineering.
13. Hibbit, H. D., and Marcal, P. V. 1973. A numerical thermo-mechanical model for the welding. *Computer and Structures* 3(11): 1145–1147.
14. Friedman, E. 1975. Thermo-mechanical analysis of the welding process using finite element method. *Journal Press. Vessel Tech. ASME*, Series J, pp. 206–243.
15. Hong, J. K., Dong, P., and Tsai, C. L. 1994. Finite element simulation of residual stresses in multipass welds. *International Conference Proceedings on Modeling and Control of Joining Processes*, ed. T. Zacharia. American Welding Society, Miami, Fla., pp. 470–476.
16. Dong, Y., Hong, J. K., Tsai, C. L., and Dong, P. 1997. Finite element modeling of residual stresses in austenitic stainless steel pipe girth welds. *Welding Journal* 76(10): 442-s to 449-s.